IEEE Access
Multidisciplinary | Rapid Review | Open Access Journal

Received 16 November 2023, accepted 17 January 2024, date of publication 25 January 2024, date of current version 12 February 2024.

Digital Object Identifier 10.1109/ACCESS.2024.3358685

RESEARCH ARTICLE

An Innovative Additively Manufactured Design Concept of a Dual-Sided Cooling System for SiC Automotive Inverters

EKATERINA E. ABRAMUSHKINA[1,2], GAMZE EGIN MARTIN[1,2], ATILA SEN[1], SHAHID JAMAN[1,2], (Member, IEEE), HAARIS RASOOL[1,2], MOHAMED EL BAGHDADI[1,2], (Member, IEEE), AND OMAR HEGAZY[1,2], (Member, IEEE)

[1]MOBI-Efficient Power Electronics, Powertrain, and Energy Solutions (EPOWERS) Research Group, Department of Electrical Machines and Energy Technology (ETEC), Vrije Universiteit Brussel (VUB), 1050 Brussels, Belgium
[2]Flanders Make, 3001 Heverlee, Belgium

Corresponding author: Omar Hegazy (omar.hegazy@vub.be)

This work was supported in part by the Electronic Components and Systems for European Leadership (ECSEL) Joint Undertaking (JU) under Grant 101007281, and in part by the research project HiEFFICIENT (www.hiefficient.eu).

ABSTRACT Modern Electric Vehicles (EVs) require high power and high efficient powertrains to extend their power range. A key element of the electric powertrain is its drive with an electric motor controlled by a traction inverter. A cooling system dissipates heat generated due to the losses in this inverter and keeps its temperature within limits, i.e. below the operational maximum value. Indirect cooling systems are often the preferred solution due to their easy implementation and robust separation of the electric/electronic parts and the coolant circuit. Indirect cooling comes with additional surface interfaces, hence thermal barriers and increased thermal resistance for the losses' heat flow path. One way to increase the system's heat transfer coefficient is by implementing power electronics with dual-sided cooling (DSC) solutions and by enhancing surface structures for the cold plates. Manufacturing complex cold plate solutions with internal surface-enhancing structures by way of classical techniques (e.g. aluminum extrusion with CNC machining) can be difficult, costly, or even not possible. Sealed one-piece solutions are preferred, without the need to weld parts or to use screws, glue, gaskets, etc. 3D metal printing allows to manufacture of a one-unit compact, light, and reliable cold plate. This study shows the advantages and limitations of a 3D metal-printed inverter cold plate by presenting the microchannel design, numerical thermal simulations, and experimental results for the liquid cooled DSC SiC and Si inverters. This work explores the compatible use of 3D metal printing solutions, which will aid the development of modern high-power density EVs.

INDEX TERMS 3D printing, additive manufacturing, dual-side cooled (DSC) module, liquid cooling, microchannels, cold plate, SiC semiconductors, automotive inverter, electric vehicles.

I. INTRODUCTION

Nowadays, the automotive industry has seen a shifting trend from Internal Combustion Engine Vehicles (ICEVs) to Electric Vehicles (EVs) to meet the environmental and energy challenges [1], [2], [3]. According to the IEA Global EV Outlook, electric vehicle stock in 2023 is more than 5 times compared to 2018 and it is over 26 million, where only 3.3 million cars are in stock in the European zone (includes EU27, Norway, Iceland, Switzerland and United Kingdom) [4]. EVs are constantly improving to higher powers, efficiency, and autonomous driving distance; as well as to lower energy consumption, weight and cost as can be seen from the Electrical and Electronics Technical Team Roadmap by the United States Department of Energy [5] and European Roadmap Electrification of Road Transport Status

The associate editor coordinating the review of this manuscript and approving it for publication was Roberto C. Ambrosio.

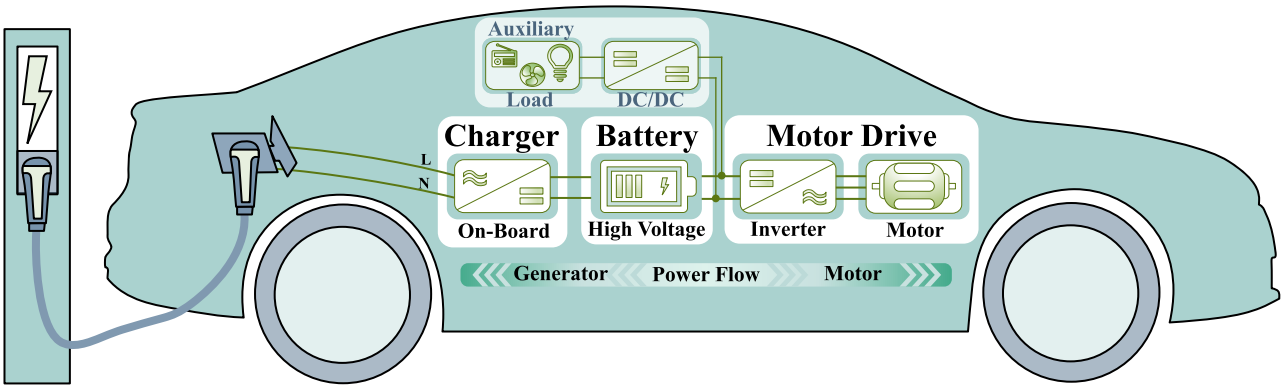

FIGURE 1. Electric vehicle propulsion diagram.

by European Road Transport Research Advisory Council [6]. Power range, efficiency, energy consumption of EVs are determined by the components of the powertrain, which includes an electric motor, a high voltage battery along with a power electronics interface: an onboard charger, a DC/DC converter and an inverter as depicted in Figure 1 [7]. The power electronics components are responsible for controlling the electrical power flow in an EV, directing it in both directions (motor mode or generation mode) between the battery and the electric motor, which serves as the propulsion system for the vehicle. All power electronics interface devices are aimed to be highly efficient, compact and reliable to improve overall efficiency and range of the EV [8], [9].

The inverter provides an energy path from DC battery side to AC motor side to control an electric motor. The most essential parts of the inverter are the active power modules, as they regulate the power flow inside power electronics devices. A power module comprises semiconductor switches, which can open and close depending on the voltage level at the gate terminal. In addition, power modules consist of not only semiconductor materials, but also electrical interconnections, a protective case, ceramic substrates, encapsulation material, etc. combined by power module packaging. All module packaging layers and their materials change power module properties, in particular, thermal resistance between the chip (more specifically its junction) and case. Modern trends in power modules manufacturing are aimed at improving module thermal performance, while lowering the module volume and weight, because of increasing demand for a high-power density device [10].

To meet the growing demand in power level and power density in power modules new advanced Wide Band Gap (WBG)-based semiconductor power electronics should be used. The WBG switches, Silicon Carbide (SiC) and Gallium Nitride (GaN), have many advantages compared to well established Silicon (Si) semiconductors: higher frequency and higher temperature operation, lower size, lower losses, because of its material properties as shown in Figure 2 [11],

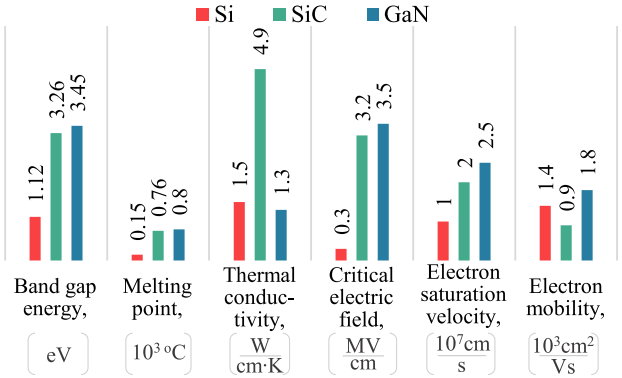

FIGURE 2. Physical properties of Si, SiC and GaN semiconductor materials.

[12]. GaN semiconductor switches are more suitable for high frequency applications because of their fast switching properties [13], [14], whereas SiC ones could be used for high-power applications such as automotive inverters, because of higher rated currents and voltages [15], [16], [17], [18], [19]. WBG converters are widely used in the EV industry according to recent studies [20], [21], [22].

To improve electrical and thermal properties for the power module, the module packaging should be optimized. The conventional power modules have electrical connections at the top and direct bonded copper (DBC) substrate for cooling at the bottom as shown in Figure 3a. Recently, a power module dual-sided packaging, which is schematically depicted in Figure 3b, has become more popular for EV applications because of lower thermal resistance and stray inductance [23], [24], [25], [26]. The DSC module has two DBC substrates (on top and bottom sides), that double the cooling surface. With increased cooling surface, thermal performance is improved, resulting in almost 40% junction temperature reduction compared to conventional power module structure [27]. Due to the improved thermal performance, the dual-side technology also provides reduced

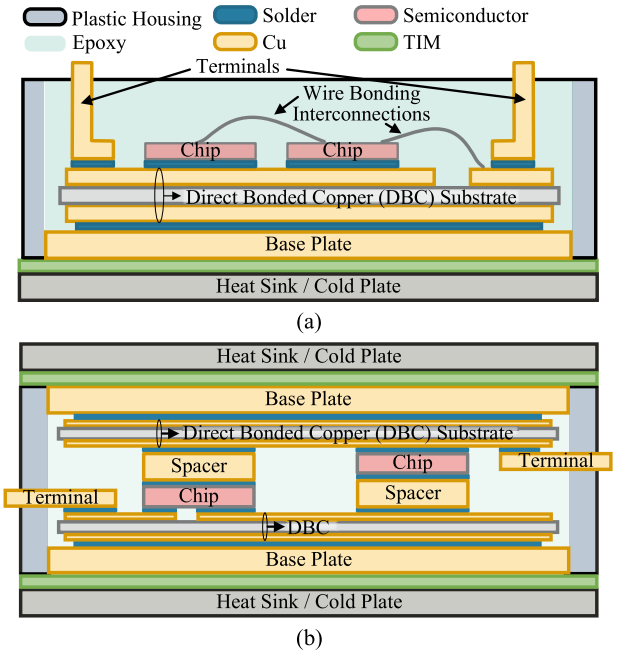

FIGURE 3. Power module structure: (a) single-sided, (b) planar dual-sided.

temperature swings and less thermal stress on the power module, which can improve the overall reliability of the considered power module. Another advantage is the absence of wire bonded interconnections as they are causing large parasitic electric parameters. In DSC modules, the wire interconnections are replaced with planar technology and connected directly to copper increasing module lifetime and improving electrical performance [28], [29].

The cooling system of power electronics devices dissipates heat from power electronics modules to provide operation below critical temperature with reduced thermal losses. All cooling systems are classified into two categories: air and liquid cooling. However, there are many approaches inside or in between these two, for example, heat pipe cooling, direct and indirect liquid cooling, natural or forced air cooling, immersion cooling, phase-change cooling etc. [30], [31], [32], [33]. Modern high-power automotive electronics mostly use liquid cooling approach because of higher heat dissipation capability [34], [35]. In direct liquid cooling approach, in principle, the thermal resistance is lower; however, implementation is complicated as extra liquid insulation is necessary. Whereas in the case of indirect liquid cooling a cold plate is placed in contact with a power module cooling surface with a thermal interface material (TIM) between them. Such a cooling approach is widely used in compact, high-power inverters as an optimized solution for EV applications [36], [37], [38], [39], [40], [41].

The manufacturing approach affects thermal and mechanical properties of the cold plate and thus, a cooling system. The cold plate internal structure defines coolant flow inside the plate as well as inner heat dissipating surface. However, the optimal internal structure could gradually improve cold plate thermal properties, the final inner design is a compromise between an optimal thermal design and manufacturing possibilities. Manufacture limitations could also lead to necessity of splitting of the design in several parts to create required inner structure, which could require the additional welding manufacturing stages. Otherwise, the leakage possibility becomes high along with increased weight and volume of cold plate as additional fixing spots required to bring parts together. Most of the commercial cooling plates are manufactured by using CNC processes in diverse ways [42]. For example, exposed tube cold plate [43], [44] has low cost and suitable for mass production, but the cold plate could not be optimized in a wide range because of tube bending radius limitations. Another approach is an aluminum extrusion [45]. In this way the cold plate is produced in separate parts, which requires a rubber gasket or additional welding to prevent leakages. Whereas a 3D printing (so-called an additive manufacturing) becomes an emerging technology for automotive cold plates or heat sinks manufacturing [46], [47]; as additive technologies allow production of an efficient and compact cold plate with fully freedom in internal structure design [48], [49], [50], [51], [52], [53]. This research focuses on overcoming manufacturing limitations of 3D metal printing to produce the cold plate in one unit. In such cold plates, lack of gaskets or welded parts improves cold plate's mechanical properties and excludes leakage possibility.

The research presents a 3D printed microchannel cooling plate design and Computational Fluid Dynamics (CFD) simulations. Experimental results are shown for the DSC liquid cooled SiC and Si inverters. The paper is divided into seven sections. Section 2 describes limitations for 3D metal printing, 3D printing manufacture considerations and the cooling plate design. Section 3 includes CFD simulations. Section 4 presents thermal performance results, a thermal model validation for SiC inverter and thermal performance comparison of SiC and Si inverters. Section 5 focuses on the main conclusions.

II. INVERTER COOLING PLATE DESIGN FOR 3D METAL PRINTING

A. INITIAL COLD PLATE DESIGN

A cold plate, in the context of traction inverters, plays a critical role for thermal management in the electric and hybrid vehicles. As the traction inverter operates, it generates heat due to the power losses as a result of power electronics switching processes. This heat needs to be dissipated efficiently to maintain the inverter's optimal operating temperature and prevent overheating. The cold plate should be made of high conductivity material, usually metal, to ensure low thermal resistance between power module and cooling liquid. The cooper cold plate will have the lower thermal resistance, however, considering high pricing, the aluminum cold plate is the optimal

choice. An aluminum cold plate is an effective solution for cooling the power electronics in the inverter module because of its superior thermal conductivity and lightweight properties.

The design and implementation of the cold plate can vary depending on different engineering considerations, for example, specific requirements for the traction inverter or the vehicle's thermal management strategy. The objectives of the cold plate design in this study is to optimize heat dissipation on the DSC power module of the traction inverter, minimize the pressure drop of a coolant inside the cold plate, decrease the overall thermal resistance of the system, perform uniform temperatures on the cases of the power modules, and ensure reliability under high power operation. The design process of the cold plate has involved careful consideration of thermal requirements, mechanical constraints, and the usage of innovative technologies such as 3D printing.

The designed cold plate has microchannels as an inner structure as microchannels enhance heat transfer efficiency, enabling rapid dissipation of high heat fluxes produced by power electronics [54], [55]. The increased surface area-to-volume ratio within microchannels reduces the thermal resistance, maintaining optimal operating temperatures and mitigating the risk of overheating-induced failures [56]. Additionally, the compact design of microchannel-based cold plates saves valuable space and weight, making them particularly well-suited for applications with limited installation space, such as electric vehicles.

As the research focuses on enabling the opportunities of the 3D metal printing, the internal design demonstrates the possibility of considered manufacturing technology, rather than on thermal optimizations. However, before the cold plate is manufactured, it is tested with a virtual setup to prove that the heat dissipation capability of the cold plate is enough for the considered power converter. The microchannels width is chosen close to the 3D printing limitations – 0.5 mm with a 0.25 mm wall between the channels. Normally, the 3D metal printing allows a minimal outer wall thickness of 1 mm and a minimum inside structure object size of 0.5 mm with tolerance within 0.2 mm. As the cold plate is designed to be built in the existing power converter the cold plate size is defined by the available space and it is 350 × 50x5 mm as can be seen from Figure 4. The cold plate's 50 mm width result in 51 channels of a 0.5 mm. After finalization of the first design idea, it is necessary to learn all of the manufacturing limitations for the chosen manufacturing method. The design should be adapted so it can be produced. These adaptations could involve major changes in the design, e.g., splitting the designed object into a few separate parts or changing the inside structure. To explain necessary changes in the design toward a manufacturable version, Subsection 2.B reviews the 3D metal printing limitations in general. Manufacturing considerations, which were done in the proposed design are described in Subsection 2.C, based on Subsection 2.B findings.

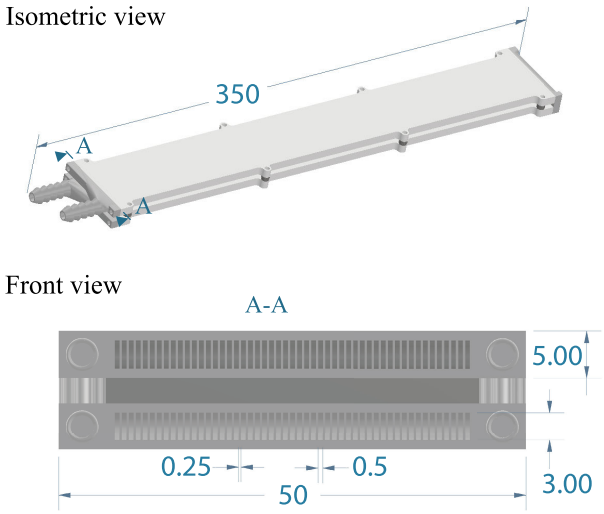

FIGURE 4. The designed 51 microchannels 350 × 50x5mm cold plate for the DSC modules cooling system: isometric and front view.

B. 3D PRINTING TECHNOLOGY OVERVIEW AND ITS LIMITATIONS

The 3D printing offers advances in prototyping speed, manufacturing complex designs, part consolidation, small batch manufacturing, and environmental benefits [57], [58], [59], [60]. In the 3D metal printing, the pre-alloyed metal powder is selectively sintered/melted using a laser following a specific pattern layer by layer. By assembling materials in such a way, intricate geometric shapes and complex material compositions can be created. In the automotive sector, the 3D printing is widely applied to prototyping, tooling, motorsports and one-offs, however, remains limited in direct digital mass production [61], [62]. Direct Metal Laser Sintering (DMLS) or Binder Jetting technologies are two main directions of the 3D metal printing [63]. However, the limitations and manufacturing processes of the 3D printing are similar for any of the 3D printing approaches; this research is focused on DMLS. This method shows material isotropic mechanical properties comparable to wrought metal material strength.

The limitations of the DMLS 3D printing technology could be categorized into overhangs and bridging. The overhangs are areas of the part that lacks a direct support from one side (Figure 5a). The maximum length of the overhang is limited to 0.5-1 mm to prevent drooping, curling or collapsing. Another limitation of the 3D printing is a bridge – a horizontal overhanging surface supported on both ends (Figure 5b). Due to the support on both ends, the bridges could have a maximum length of up to 2 mm. Considering manufacturing of hollow components those lengths are little. There are two main approaches to extend the length: adding support structures or changing the printing angle.

The support structures (Figure 5c) could not only increase the allowed length of overhangs and bridges, but also stabilize the part on the platform, dissipate excess heat, and prevent

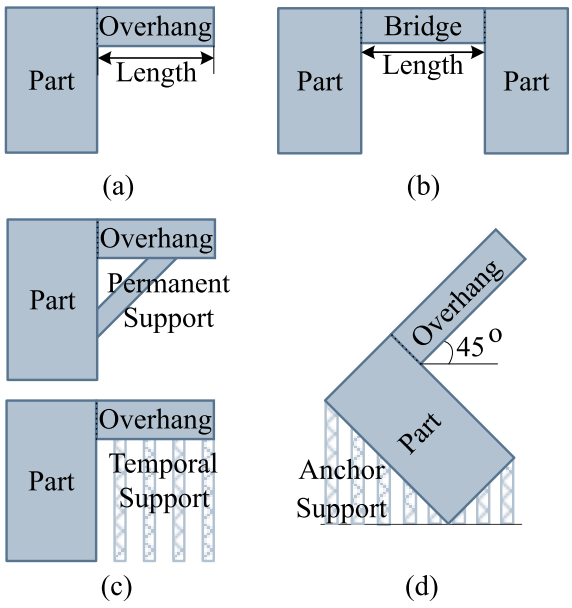

FIGURE 5. 3D printing objectives: (a) overhang, (b) bridge, (c) support, (d) printing angle.

warping. Besides, the support could serve as an anchor on the build plate, preventing upward curling of a material caused by thermal stress. The support could be temporary and permanent (as a part of the design). All temporal supports are supposed to be removed at post-processing stage by grinding or sandblasting. Another way to increase the overhang or bridge length is to adjust a printing angle. For example, in Figure 5d the horizontal overhang can be printed without any support underneath it, as the whole part has an angle of 45° to the baseplate. In this case, overhangs or bridges inside the part could be printed, despite it being impossible to place a temporary support.

The 3D printing could potentially enhance the cooling systems for EV components according to recent studies. For example, researchers have designed 3D printed heatsink structures with optimized geometries, offering superior heat dissipation capabilities for battery packs and power electronics [64], [65]. The cold plates for indirect liquid cooling have internally a hollow structure, which in case of the 3D metal printing, is limited to the 1-2 mm width channels. In recent studies, this limitation is avoided by slitting the design in two or more parts [66]. However, in this case the manufacturing can be done with, for example, an aluminum extrusion, and makes the 3D printing an unjustified choice. On the other side, open structures such as heat sinks could be easily 3D metal printed because there are no internal bridges and overhangs [67], [68]. Another way to avoid mentioned limitations is to use a 3D polymer printing where possible, as the 3D polymer printing limitations are different due to lower material weight compared to metal. In the case of a direct liquid cooling, as the power modules are in direct contact with the coolant, it is possible to print a polymer heat sink and limit heat dissipation by contact area of the heated surface with the liquid coolant [69]. For the indirect liquid cooling a polymer cold plate or heat sink are not compatible solutions as the heat dissipation occurs through the cold plate wall. The cooling plate, which is printed in a few units, requires additional parts welding manufacturing stage or additional mechanical connections (e.g. a rubber gasket and screws), adding weight and volume and lowering reliability as each joint could cause a leakage. To fully use the advantage of 3D printing, the metal cold plate design should be improved to allow printing the cold plate in one unit.

C. CONSIDERATIONS FOR A COLD PLATE DESIGN FOCUSED ON 3D METAL PRINTING

The 3D printing has the limitations obliging to compromise between a thermal optimized design and a design which is manufacturable. The main findings in improving the cold plate design towards a 3D printing manufacturable design are discussed from different points of view. For example, for the 3D metal printing, the metal has powder initial state, which provides the specific material structure and affects mechanical properties of the final part. As the metal powder particles are sintered together at high temperature, metal parts could melt unequally, different defects could emerge inside the metal structure. One of the important defects is a hole through the cold plate wall. Based on practical experience with previous prototypes, it was decided to keep cooling plate walls thickness 2 mm or slightly more, to ensure continuous surface of the cold plate outer wall. Another consequence coming from the powder origins of printing material is that the surface texture is grained. For the indirect cold plates, the contact surface should be flat to ensure close contact between the cold plate and the power module (heat source). This defect could be eliminated at the post-processing stage by polishing the contact surface. However, in that case the initial wall thickness should be increased to compensate polishing.

The layer-by-layer production process requires a support to layer metal powder. This makes the cold plate nostril design one of the challenging steps in the cold plate design as the hollow nostril creates a non-supported and impossible to print ''bridge''. For the developed design, this limitation is resolved by printing a cold plate vertically to minimize ''bridging''; and by adding permanent support to the design for each liquid channel as presented in Figure 6 to avoid little ''bridges'' created by cooling channels walls. This modification in the design would not affect thermal performance but allow to print the cooling plate in one unit, including a nostril.

In addition, another challenge related to overall design is that the microchannels cold plate design implies long and narrow channels as part of the inside structure. For the 3D metal printing, the narrower and the longer the microchannels are, the higher the possibility of channels' internal collapsing. At the same time, apart from the possibility of internal collapsing, long and narrow liquid channels increase inner

pressure drop regardless of the manufacturing approach. Based on that, to avoid collapsed channels and high inner pressure, the cold plate length should be as short as possible. Besides, the long and thin plate could be easily bent requiring additional assembly holes (and screws) placed along the length to ensure close contact between the cooling plate and the power module.

III. VIRTUAL SETUP THERMAL PERFORMANCE ASSESSMENT OF DUAL SIDE COOLED SIC TRACTION INVERTER

A. VIRTUAL SETUP DESCRIPTION

Thermal performance of the designed cold plate is investigated by carrying out a series of the CFD simulations using ANSYS® Fluent. These simulations are aimed at evaluation of cooling effectiveness through a forced liquid cooling method. The coolant (water or water/glycol) flows through the microchannels of the aluminum cold plate to efficiently dissipate heat generated by the DSC module. To ensure efficient analysis, the initial step involved simplifying the cold plate geometry in Ansys Design Modeler, and removing unnecessary components (e.g., screws) from the simulation setup. The refined simulation model allows one to focus on key aspects and critical features that influence the cooling performance whereas minimizing computational overhead. As can be seen from Figure 7, the model consists of a cold plate, a coolant and the DSC modules.

The following simulation stage is a meshing process, which discretizes the physical model into multiple parts and facilitating the application of the mathematical model in ANSYS® Fluent. The meshing subdivides the complex geometry of the cold plate into a structured network of elements and nodes, enabling precise numerical simulations for fluid flow and heat transfer analysis. The final mesh configuration consisted of approximately 16 million elements and 5.3 million nodes, ensuring a highly refined representation of the cold plate's intricate features and increasing the accuracy of the CFD simulations.

The next step following the meshing initiates simulations in ANSYS® Fluent. To enable accurate and realistic analyses, specific material properties shown in Table 1, have been assigned to the various layers of the DSC module. In Figure 8, each layer represents a distinct component of the DSC module, such as TIMs, spacers, Silicon Carbide (SiC) chips, solders, and substrate layers (copper and ceramic) [70]. By assigning appropriate material properties to these individual layers, their thermal behavior during the simulation process has been accurately modelled.

The CFD simulations have been performed to analyze the fluid flow and heat transfer characteristics within the microchannels of the cold plate. By considering various operating conditions such as the coolant temperature and coolant flow rates, valuable insights into the heat dissipation capabilities and thermal uniformity of the cold plate design have been aimed to gain. The cooling system for electric vehicle powertrain generally has coolant temperature of 65 °C and coolant flow rate 12 liter per minutes (l/min) in the cooling loop [24]. Because of the lab availability, the cold plate could be tested at coolant temperature equal to ambient temperature, which is around 25 °C inlet and at a flow rate 2 l/m. To analyze the trend in junction temperatures depending on inlet temperatures and inlet flow rate, the simulations are made for 25 °C and 65 °C coolant inlet temperatures and for the range from 2 to 12 l/m coolant flow rate. In this case, the simulation model could be validated at 2 l/m and 25 °C inlet flow; and after that could be evaluated at worst case scenario, i.e. 12 l/m and 65 °C inlet flow. As a part of the boundary condition, different heat losses levels are simulated including maximum heat loss per chip, which has been calculated by considering maximum total amount of losses per module mentioned in a datasheet.

TABLE 1. Thermal properties of the layers of the model.

Layer	Thermal Resistance ($^oC/W$)
Thermal Interface Material (TIM)	0.0157
Copper	0.0004
Ceramic	0.0071
Chip + Spacer + Solders (in total)	0.9056

B. SIMULATIONS RESULTS

After applying the specified boundary conditions to the model, the simulation process was iteratively refined under steady-state conditions. Figure 9 shows the result of the condition that the inlet coolant temperature of 25 °C, the coolant flow rate of 2 l/min and the total heat loss of 800 W on the entire system of 3 power modules in inverter configuration. The chosen total heat loss of 800 W corresponds to maximum heat loss level expected later at the experiments stage. The maximum reached junction temperature is 67.8 °C as shown in the temperature distribution of the entire system and modules in Figure 9. Figure 9a shows temperature distribution of the entire system, whereas temperature distribution for different modules are shown in Figure 9b. This temperature profile offers valuable insights into the thermal behavior of the components, highlighting potential areas of concern and enabling design adjustments to effectively manage temperature-related challenges. Figure 9d and Figure 9c provide details regarding the fluid dynamics within the system. In Figure 9c the red colored zone represent the higher pressure. In this zone, the registered pressure drop reached maximum 11.5 kPa (equivalent to 114.6 mbar), which indicates the resistance encountered by the coolant as it flows through the system. Furthermore, the achieved maximum flow velocity attains 3.22 meters per second (m/s) where the pressure drop takes its lowest values. At the inlet, where the pressure reach maximum value, the initial inlet flow velocity is 1.88 m/s at the flow rate of 2 l/min.

Further CFD simulations have been conducted using ANSYS® Fluent. The objective is to investigate the impact

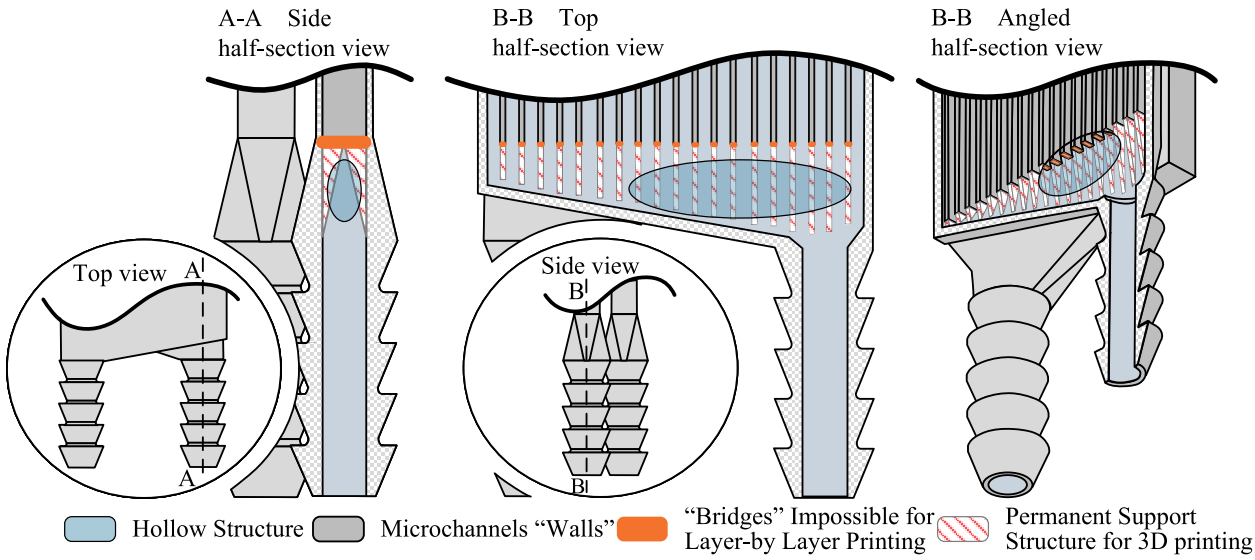

FIGURE 6. Permanent support for microchannel printing.

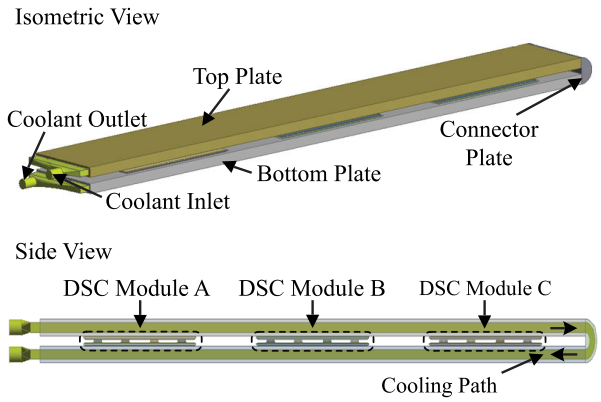

FIGURE 7. The refined simulation model: isometric and side view.

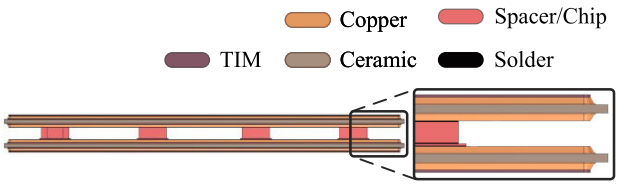

FIGURE 8. The DSC module model: module side view and module layers.

of varying coolant flow rates on both pressure drop and temperature performance of the cold plate. Figure 10 presents the results for 800 W heat loss at different low rates staring with 2 l/min. The highest chip junction temperature at various flow rates is show in Figure 10 in a red color, where 25 °C inlet coolant temperature is indicated by solid line and 65 °C by a dashed one. The corresponding coolant pressure drop at various flow rates is shown by a solid line in a blue color. The simulation demonstrates that although augmenting the flow rate leads to a significant increase in the pressure drop, the temperature profile shows a certain variation (approximately 6 °C). This increase in pressure drop depending on flow rate is explained by microchannels internal structure of cold plate, as the microchannels have only 0.5 mm width. As a result, the system behavior becomes close to jet impingement system which can operate at flow rates around 0.5 - 2 l/m [71].

Considering these findings, additional CFD studies have been conducted using Ansys Fluent to evaluate the performance of the cold plate under diverse operating conditions. These conditions have involved two coolant inlet temperatures, i.e. 25 °C and 65 °C, as well as two different heat loss levels. One is another heat loss level expected at the experimental stage to be used later for simulation model validation. And the other is the maximum heat loss level to evaluate power modules temperatures at worst-case scenario. By conducting these additional simulations across a range of conditions, a comprehensive understanding of the thermal capabilities and limitations of the cold plate has been achieved. The results are shown in Figure 11, where the maximum junction temperature reached on the chip of each module calculated at the flow rate of 2 l/min. Module A shows the highest temperature at the 25 °C inlet temperature and Module C at 65 °C because of module's spatial arrangement withing the system. When the coolant temperature is lower, a temperature difference exists between the inlet and outlet points, significantly impacting Module A due to its proximity to both points. Conversely, at higher coolant temperatures the temperature difference at the inlet/outlet points is lower, which causes a less thermal optimal position for a Module C – remotely from the inlet and outlet points. The observed thermal behavior underscores the intricate interdependence between coolant temperature, spatial positioning, and heat distribution within the system. At low heat losses (500 W), the low variation among modules within

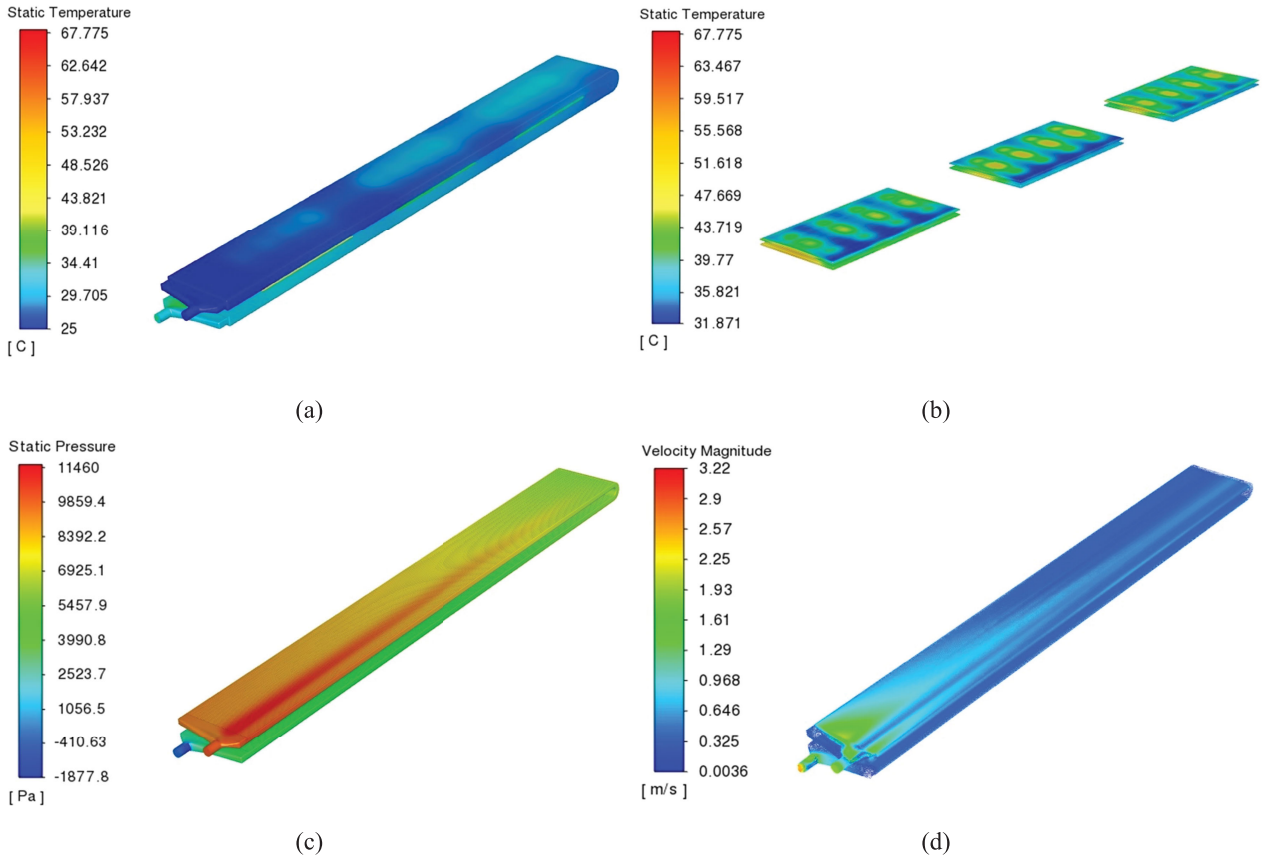

FIGURE 9. CFD simulation results (a) temperature distribution of the entire system; (b) temperature distribution of the modules; (c) the flow profiles for pressure drop and (d) the flow profiles for coolant velocity.

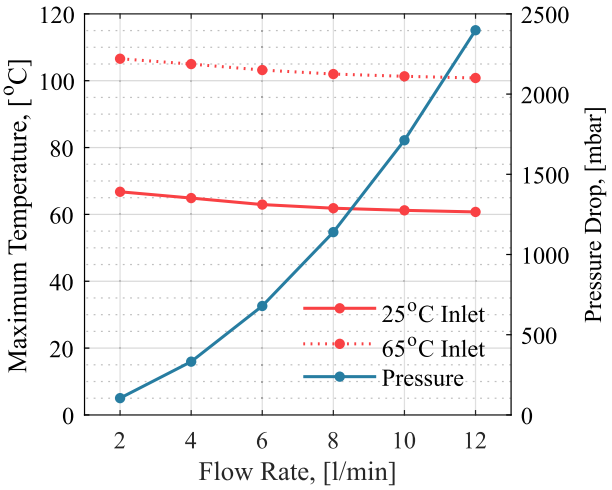

FIGURE 10. Maximum junction temperature and pressure drop results at different flow rates at 800 W heat losses.

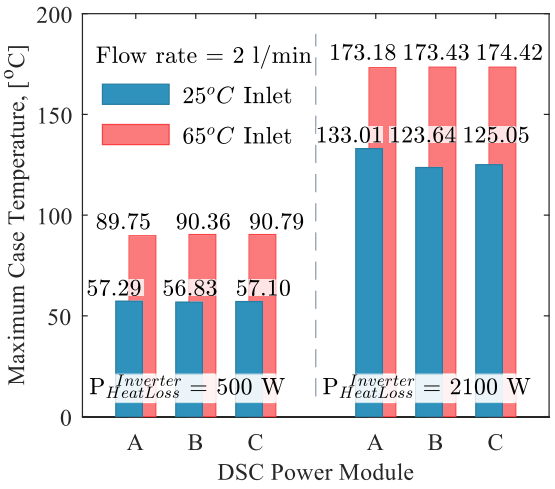

FIGURE 11. Maximum junction temperature at different heat losses for the coolant temperature of 25°C and 65°C at the flow rate of 2 l/min.

each scenario (around 1 °C) explained by relatively low temperatures of power modules.

In the most challenging scenario – a flow rate of 2 l/min, a coolant temperature of 65 °C, and a substantial heat loss of 2100 W — the calculated maximum temperature on the chip is 174.42 °C. This value is rather close to the critical threshold of 175 °C, however, as can be seen from 10, at a higher flow rate, the maximum temperature can drop. With the maximum flow rate 12 l/min, the temperature could be around 5 degree lower, which represents 5 °C margin to the

TABLE 2. Infineon SiC MOSFET module prototype properties.

Parameter	Value
Module size, (mm)	50x40x3
V_{DS}, (V)	1200
I_D, (A)	400
$T_{junctionMAX}$, (^oC)	175

upper operational limit for DSC modules during switching states at maximum operating inverter power. This careful temperature management ensures the chip's optimal function and sustained operation within its intended parameters. This approach not only contributes to a resilient and enduring system, but also guarantees the overall stability and reliability of the setup.

To summarize, the presented sequence of CFD simulations is aimed at evaluating the thermal performance of the cold plate. The design exhibits enhanced heat dissipation capabilities, compact advantages, and cooling uniformity. All the advantages significantly contribute to extending the lifespan and increasing the reliability of cooled objects, i.e., power electronics components. The simulations result demonstrate that the cold plate is ready for laboratory-based validation under real operational conditions. This transition from simulations to practical testing is a necessary step towards confirming the cold plate's thermal performance and its applicability in real-world scenarios.

IV. EXPERIMENTAL THERMAL VALIDATION FOR DUAL SIDE COOLED SIC AND SI TRACTION INVERTERS

A. TEST SETUP FOR DUAL SIDE COOLED SIC TRACTION INVERTER

The cooling system is tested with a power electronics converter with an inverter topology. The schematic diagram of the test setup is shown Figure 12. The designed cooling plates dissipate heat from the exclusive DSC half-bridge MOSFET SiC module prototypes, which are provided by Infineon for testing [72]. The power module image could be found in Figure 12 and module properties are in Table 2.

A test setup is shown in Figure 13a [73]. The test setup is established by connecting a high-voltage battery emulator to the input of an inverter and a three-phase RL load to the output. The DC link includes 10 film capacitors of 85 μF connected on the DC side of the converter, as shown in Figure 13b. Two snubber capacitors of 220 μF were connected at the drain source of each half-bridge module.

Analog voltage transducers (DVC 1000-P) and current transducers (LEM LF 305-S) were used to measure currents and voltages on both the DC and AC sides of the inverter. A control technique of a three-phase inverter is implemented by employing a sinusoidal modulation index. To generate Pulse Width Modulation (PWM) signals, a real-time controller is implemented into the dSpace MicroLabBox®. The dSpace Graphical User Interface (GUI) was designed in the Controldesk software to provide reference commands, signal visualizing and measurement. All experimental data was logged in to the computer database.

TABLE 3. Infineon SiC MOSFET module prototype properties.

Parameter	Value
Type	Indirect Liquid Cooling
Chiller	380 mm Radiator & Forced Air
Flow direction	Series Flow
Flow rate	2 l/m
TIM	T-flex 600 & 6000, 3 kW/K
Distance between modules	50 mm
Coolant liquid	Water

The cooling system parameters, including a Thermal Interface Material (TIM) material, flow rate etc. are presented in Table 3. The TIM was used on both sides of each module (top and bottom) between the module and the cooling plate. The cooling water has series flow, meaning flowing from the first module (counting from the inlet) to the second and the third, then the flow returns in a backward order (3-2-1). The water loop is provided by a lab-made chiller with a built-in radiator, a water tank and a pump.

To measure the case temperature, the K type thermocouples were placed between the module case surface and the TIM layer on the top side of each module. All temperatures were recorded using the Labfacility L200 temperature logger. The Labfacility L200 can provide 8-channel temperature measurement, scanning and logging of measured values. It can also be used as a stand-alone indicator and incorporates a digital display of measured temperature. Apart from thermocouples, to detect thermal performance a thermal infrared camera was installed to film the inverter from the top side.

B. EXPERIMENTAL RESULTS AND VALIDATION FOR DUAL SIDE SIC TRACTION INVERTER

The converter was tested in inverter mode with open-loop Space Vector PWM control at 10 kHz switching frequency. At a 400 V DC-link voltage, maximum testing power reached 41 kW level due to lab equipment availability. To evaluate thermal performance, case temperature and efficiency measurements, together with thermal camera images were recorded. Case temperature depending on input power are shown in Figure 14a and thermal camera image at maximum testing power 41 kW in Figure 14b.

The key point of evaluating power electronics converter cooling system is to conclude whether it keeps the temperatures of power electronics devices under maximum working temperature. To fully answer this question, the cooling system should be tested at worse case conditions, for example maximum working power, higher temperature of inlet coolant liquid etc. However, it is also possible to use experimental data for validation of a virtual prototype. Because of the lab limitations the converter was tested only at 41 kW power level, which is around 30% of maximum power. As can be seen from Figure 14, the maximum case temperature raised

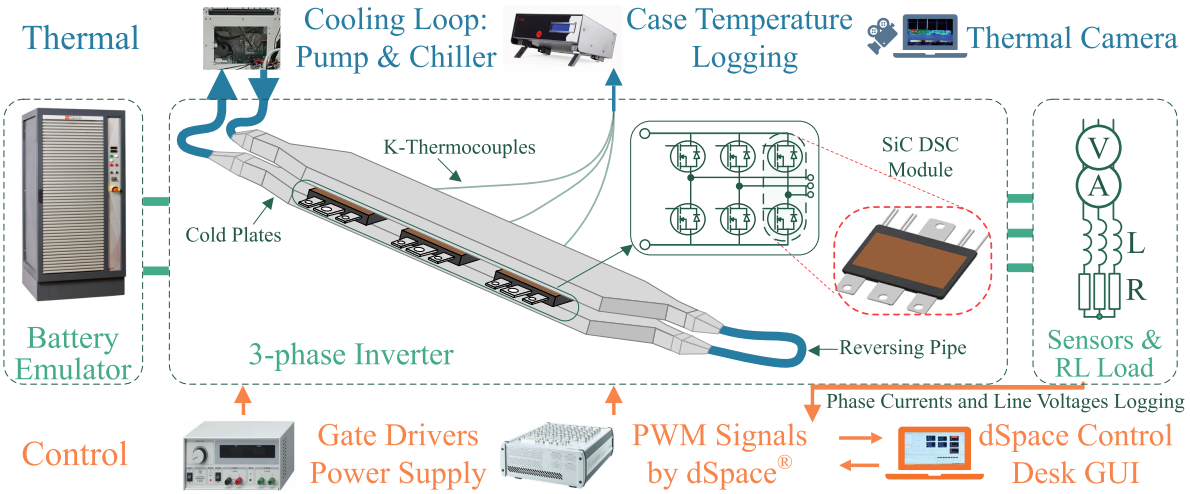

FIGURE 12. Dual-side cooled three-leg traction inverter experimental setup diagram.

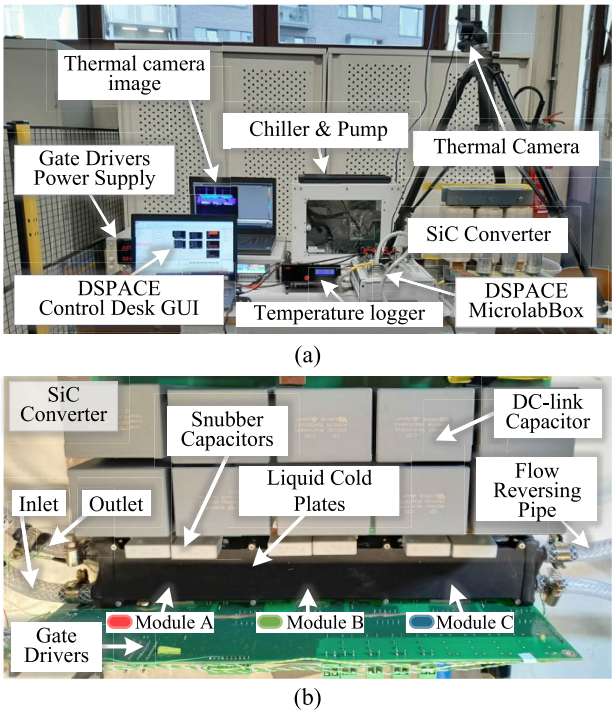

FIGURE 13. 150 kW SiC traction dual side cooled inverter test setup: (a) setup overview (b) inverter and cold plates.

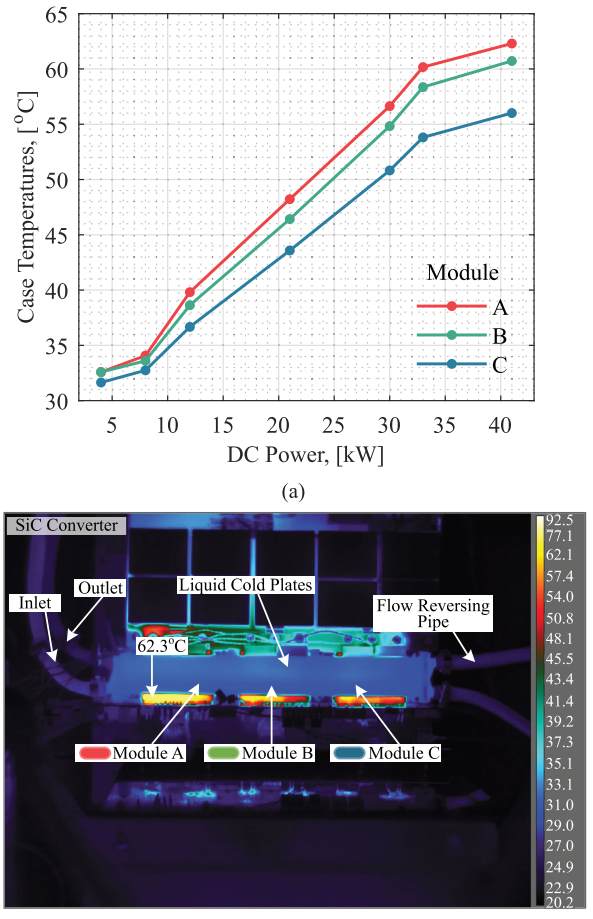

FIGURE 14. SiC inverter thermal experimental results: (a) DSC module heatsink temperatures. (b) Experimental infrared thermal camera image of the inverter at 41 kW.

up to 62.3 °C at maximum testing power (41 kW). It is 35% of the maximum working temperature range of the modules, which matches the testing power level. Tested inverter power levels considered a low power region, where the efficiency of the inverter is increasing as can be seen from efficiency map depicted in Figure 15. The efficiency will rise and stabilize, when the power level is at least 50% of maximum inverter power.

The virtual prototype validation includes recreation of test conditions in simulation environment and comparing simulation results with experimental data. As can be seen from Figure 16, simulation temperatures are close to simulated values. The temperatures in the experiment are lower because of a liquid coolant chiller in the cooling loop. The chiller introduces additional pressure drop in the system, which wasn't considered at the simulations stage. This additional pressure drop is causing lower temperatures

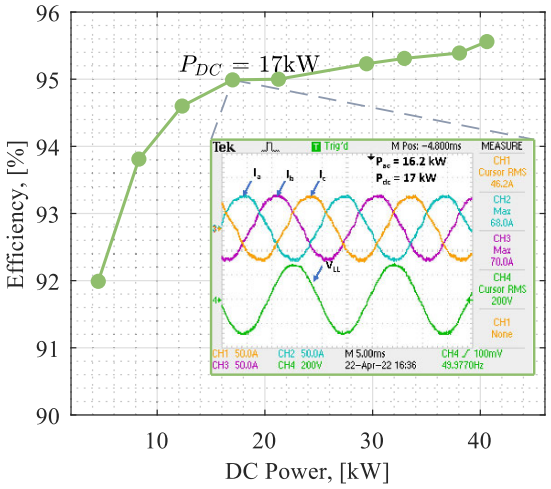

FIGURE 15. Experimental three-phase SiC DSC inverter efficiency map and load currents and voltage at 17 kW.

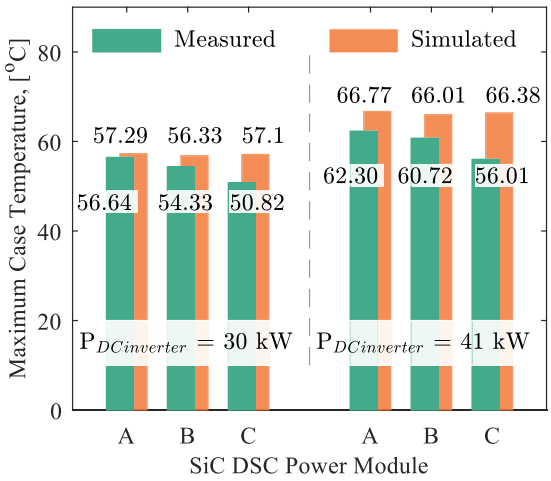

FIGURE 16. Experimental thermal validation results.

compared to simulations as well as uneven temperatures between power modules. Nevertheless, the simulation model shows high convergence with experimental results. After validation of the simulation model, normally, the worst-case scenario is simulated to evaluate whether the designed cooling plate could be used in a wide power range. The worst-case simulations are shown in Section 3 in Figure 11, where maximum junction temperature of the power electronics devices stays under the maximum working temperature value. Thus, at higher power level the cooling system will dissipate enough heat and the power module temperatures will stay under maximum working temperature, which is 175 °C for considered module; and the designed dual-sided cooling plate is capable ensure working conditions for considered converter.

C. THERMAL PERFORMANCE COMPARISON BETWEEN SIC AND SI TRACTION INVERTERS

Recently introduced to the market WBG semiconductors undoubtedly have advanced physical properties promising better thermal and electrical performance of WBG

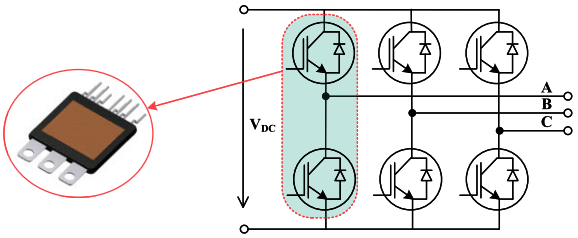

FIGURE 17. Si dual-sided module: 3D model and inverter topology.

TABLE 4. Infineon FF400R07A01E3_S6 Si Power Module Properties.

Parameter	Value
Module size, (mm)	42x42x3.5
V_{CEs}, (V)	700
I_C, (A)	400
$T_{junctionMAX}$, (^oC)	175

semiconductor devices. At this moment many research and companies are trying to draw a bigger picture of WBG's promising properties and show the real experimental results showing operation performance of WBGs [15], [16]. To contribute to this part of power electronics research the designed cooling plates were tested with Si IGBT (Insulated Gate Bipolar Transistor) dual-sided modules as well. The performed experiment tests SiC MOSFET module and Si IGBT module under the same conditions to compare thermal performance.

For this test, the same 3-phase voltage source inverter topology was used. The topology and a picture of the module are depicted in Figure 17. The dual-sided Si IGBT half-bridge module properties are presented in Table 4.

The Si IGBT and SiC MOSFET converters are tested at the same power levels with the same load. All of the measurement and data acquisition devices are the same as can be seen in Figure 18a. The Si IGBT setup is specially designed for this thermal performance comparison test. Because of using a bent DC-link busbar, the DC-link capacitors are placed under inverter switches and surrounding switches cooling plates, making the prototype a compact device as shown in Figure 18b. The inverter size is 240 × 320 × 160 mm. Considering the maximum operating power of 120 kW the power density is 9.7 kW/L. The DC link includes 2 film capacitors of 4700 μF. For each inverter, a snubber capacitor 1500 μF is used. To send PWM signal standard gate drivers were used, but it is also possible to use a commercial gate driver for this module.

A thermal performance comparison is done based on two objectives: measured case temperatures of Module A and efficiency. Both converters are tested at four different power levels: 4, 8, 12 and 16 kW. As shown in Figure 19a case temperatures of Si IGBT module are rising about 1.5 times faster than it is for SiC MOSFET module, and the efficiency of SiC is higher than for Si IGBT at considered power levels. This difference is explained by physical properties of SiC semiconductors presented in Figure 2. For example, SiC semiconductors have higher band gap energy, i.e. wider band gap. A wide band gap requires electron to have more energy

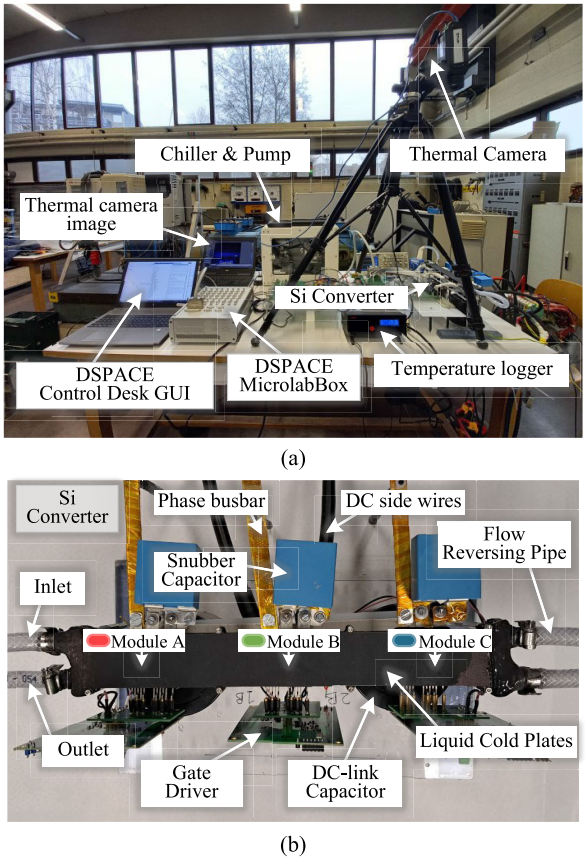

FIGURE 18. 120 kW Si traction dual side cooled inverter test setup: (a) setup overview (b) inverter and cold plates.

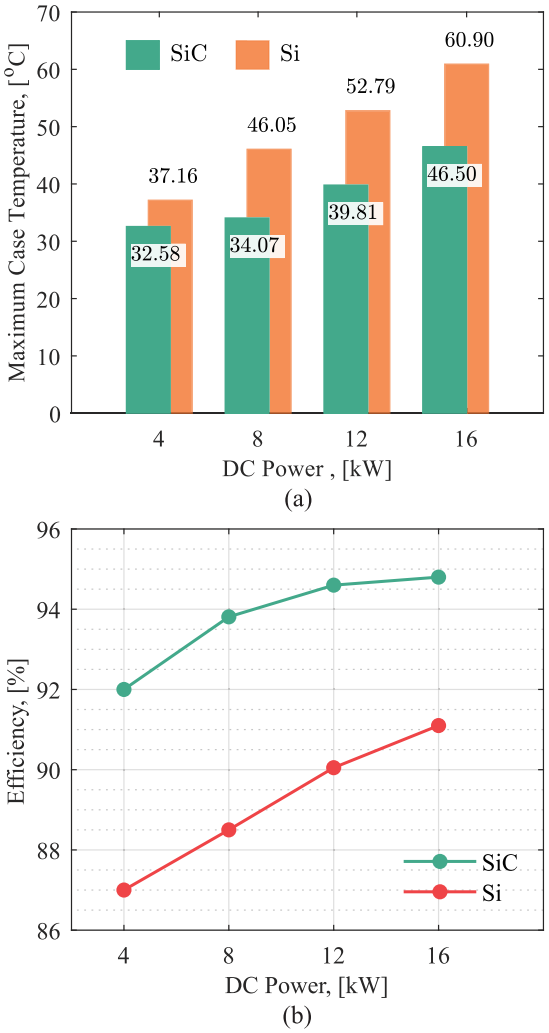

FIGURE 19. Thermal comparison results: (a) temperature comparison for Module A (b) efficiency map.

to come from valence band to conduction band. Thus, when the band gap is shrinking under high temperature or high voltage conditions, the WBG semiconductors it is less critical than for Si resulting higher efficiency of SiC semiconductors. In addition, the thermal conductivity of SiC semiconductors is around 3.4 times higher than for Si. That means, SiC module will have lower thermal resistance and, consequently, lower temperature than Si, whereas the module packaging and cooling system is the similar. The presented results show advanced thermal and electrical performance of SiC power module compared to Si. However, the results should be interpreted with caution due to Si IGBT module is rated for almost halved DC voltage. It is possible that for modules rated at the same voltage and current level the difference could be smaller. Nevertheless, as both switches are tested at low power levels compared to their maximum allowed power, the difference in rated voltages should make less impact. The efficiency comparison depicted in Figure 19b as can be seen, at the same power level Si power module has more losses than the SiC with the same cooling conditions.

V. DESIGN CONSIDERATIONS AND BENEFITS FOR 3D METAL PRINTED COLD PLATES FOR POWER INVERTER

This study investigates benefits and limitations of the 3D printing manufacturing approach for the power converter cold plates. The 3D printing allows to create a cold plate design matching with the heat generator size and custom arrangements of cooling channels, including microchannels or channels generated by AI (Artificial Intelligence). That opens a wide range of possibilities to create compact devices, which could be built in any system whereas taking minimum space. With rising demand for highly effective cooling systems for the automotive power electronics, the 3D metal printing technology suggests design opportunities. However, includes its own limitations, which are crucial for the internal structure of the indirect liquid cooling. For example, the inner hollow structures of 3D metal printed parts are currently limited to maximum 2 mm length. This limitation creates an additional challenge in indirect cold plates design because of cooling channels form the hollow structure inside the plate.

The two-step approach is developed to overcome the 3D printing limitations. The first step is to optimize the printing angle to create minimum unsupported surface placed at angles less than 45^o with the printed surface. At first, three placements were considered for the designed cold plate, as shown in Figure 20a. The placement number III was chosen for the design as in this case only the beginnings of

TABLE 5. The comparison of cooling plates designed and produced in diverse ways.

Ref.	Manufacture method	Features	Advantages & Disadvantages
[37] [50] [55] [54]	Machining of an aluminum block including drilled holes.	The rectangular cooling plate with channels is made in two parts: top and bottom joint, welded or screwed.	Advantages: • The design is ready to be manufactured with available methods at low cost; • The design can be thermal- and size-optimized; Disadvantages: • The need to join two units by adding welding manufacture stage or by screwing, which increases the possibilities of leakage whereas decreasing the system's reliability and mechanical stability.
[44]	CNC machining including buried pipe process and multi-step welding.	The rectangular exposed tube cold plate: the copper pipeline circulates through the rectangular aluminum closed cavity.	Advantages: • Increased reliability as the cooling plate is manufactured in one unit – no additional welding or screws and gaskets are needed; • Suitable for mass production; • High dissipation efficiency, small thermal resistance; Disadvantages: • The cost is higher compared to machining of an aluminum block; • The bending radius of the tube affects thermal performance; • The shape of a cold plate is limited to rectangular.
[41]	Metal wire-arc thermal spray deposition technique.	The custom-shaped liquid channels cooling plate is produced in one unit by involving complex manufacture process. Liquid channels are formed with dissolvable PVA insert.	Advantages: • Increased reliability as the cooling plate is manufactured in one unit – no additional welding or screws and gaskets are needed; • The design can be thermal-, size- and weight-optimized; • Unique idea of forming liquid channels is implemented; Disadvantages: • Complex manufacture process: 6 step process including pre-machining, metal spraying and post machining along with separate production of matching PVA insert.
This design	3D metal printing	The microchannels liquid cold plate is 3D printed in one unit.	Advantages: • Rapid prototyping is possible; • Mechanical properties of 3D printed metals are comparable with original metals; • Production process includes only a 3D printing stage and a final polishing; • Possibility of custom arrangement of inside structure including GA optimized structures; • The design can be thermal-, size- and weight-optimized; • Increased reliability as the cooling plate is manufactured in one unit – no additional welding or screws and gaskets are needed; • Permanent supports, which are added to the design for 3D printing purposes, do not affect cold's plate thermal performance; Disadvantages: • The price is higher than for exposed tube cold plate or exposed metal block approaches. • The design should be optimised for the 3D metal printing.

the cooling channels separation walls are unsupported and parallel to the printing surface (marked orange in Figure 20a). The second step in the developed approach is to create the permanent supports inside the plate in such a way that all surfaces will compose angles equal or greater than 45^o with the printing surface. The designed permanent supports are placed as shown in Figure 20b to create 45^o with the printing surface.

As a result of applying the suggested method, the designed cold plate could be printed as one unit including the main body with inlet and outlet nostrils. To be 3D printed, the designed cold plate has permanent internal structures as a part of the internal structure, which do not affect thermal performance of the plate. The proposed design has numerous advantages compared to cold plates manufactured with traditional approaches. The 3D metal printing technology allows rapid prototyping whereas mechanical properties of the 3D printed metals are comparable with the original metals. The production process includes only 3D printing and post-machining polishing stages. Regarding the cold plate, polishing is necessary for surfaces which are in direct contact with heat sources to ensure close contact and lower thermal resistance.

The traditional manufacturing approaches are machining of an aluminum block and an exposed tube. Regarding the machining of an aluminum block approach, the main disadvantage is implying at least two-unit cold plates with the necessity of joining two parts together by welding or by additional assembly, e.g. resin gasket and screws. However, such an approach allows to optimize the internal structure of the cold plate. As for the exposed copper tube cold plate; although, the thermal resistance such a plate

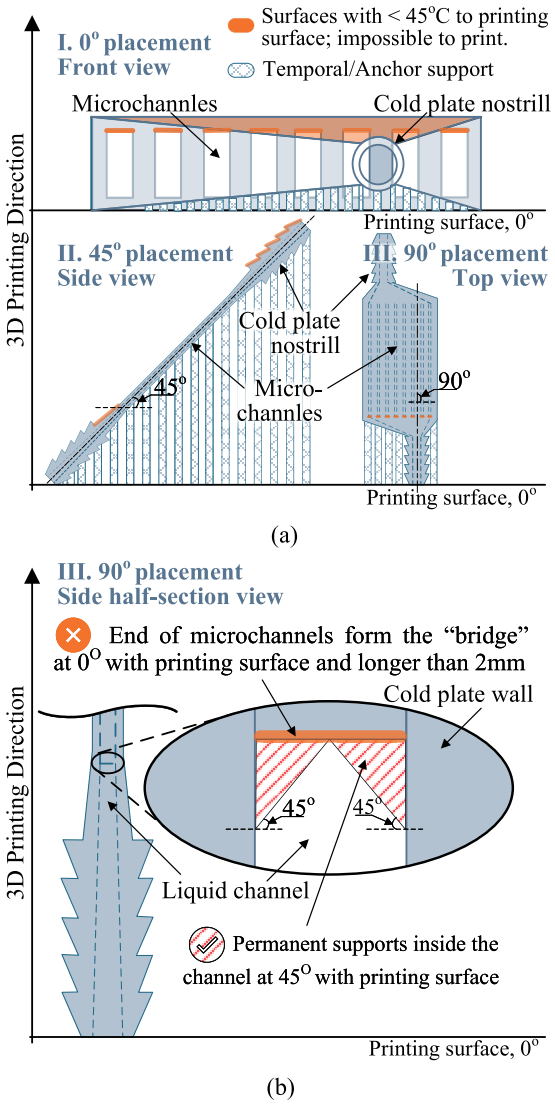

FIGURE 20. Suggested approach to overcoming 3D printing limitations approach: (a) printing angle optimization (b) Adding permanent support structures.

is low because of copper' high thermal conductivity; the final cold plate shape is limited to rectangular, and the internal structure is constrained by possibilities of copper tube bending. Compared to the traditional manufacturing methods, the 3D printing allows a cold plate optimization to minimize the volume and weight, and to integrate the device into the system; as well as to optimize the inner structure and create custom liquid channels, pin-fins etc. The unit package of the cold plate eliminates the need for a resin gasket for the water insulation and gasket assembling screws. The lack of resin gaskets eliminates the possibility of leakages and makes design less complicated, lightweight and compact. A detailed comparison of manufacturing method for cold plates is presented in Table 5.

VI. CONCLUSION

The study shows a 3D printed cooling plate design for the indirect liquid cooling systems for an automotive inverter, including the 3D metal printing limitations overview and the development of virtual prototype experimental validation. The inverter dual-side cooling system consists of two identical cooling plates: for heat dissipation from top and bottom sides of the dedicated dual-sided power modules. Experimental results and validation are presented with a new WBG SiC MOSFET power module. Dual-sided contact packaging increases cooling surface of the module and reduces overall module thermal resistance. To evaluate thermal performance of SiC compared to well established Si semiconductor material, the thermal test of the cooling plates is also performed for Si IGBT switch type of dual-sided cooled power electronics modules. SiC semiconductor power modules showed improved thermal performance as was suggested from physical properties of WBG semiconductors.

The research develops an approach to adapt the cold plate design to avoid the 3D printing limitations. The two-step approach includes printing angle optimization followed by integrating internal permanent supports in the design. These integrated supports become part of the internal structure and have no effect on thermal performance. Because of the applied changes to the design, the cooling plate is printed in one unit, and the design does not require additional welding or assembly with resin gaskets and screws. The one-unit plate has increased mechanical strength and reliability as leakage possibilities are decreased. Moreover, absence of additional assembly holes with screws is lowering system weight and volume. Besides, the 3D printed cold plate could have inner structure or outer wall of down to (sub) millimeter widths, which is another factor in reducing overall weight of the device is the capability with 3D printing. The 3D metal printing opens new opportunities for a cold plates production, such as a rapid prototyping cycle; reduced device/system volume and weight; and the possibility of custom cold plate internal structure design with fine cold plate structures.

This work focuses on the limitations and benefits of the 3D metal printing. The future work is planned in two directions. The first direction is to develop the proposed approach and design fully thermal-optimized 3D printed cold plate reaching better compromise between thermal behavior and manufacturability of the cold plate. The thermal optimization includes cold plate geometry modifications, e.g. an optimal channel width and length, an optimal cold plate length, the inlet/outlet nostrils diameters etc. Another direction is related to the applying the developed approach to the design of a direct liquid cold plate. From the 3D manufacturable design point of view, the direct cold plate has the same problem with printing hollow structures close to inlet/outlet nostrils. The difference will be in missing outer wall at the side on power module, which should have direct contact with liquid coolant.

ACKNOWLEDGMENT

The authors acknowledge Flanders Make for the support to the MOBI Research Group. The JU receives support from the European Union's Horizon 2020 Research and Innovation

Program and Austria, Germany, Slovenia, Netherlands, Belgium, Slovakia, France, Italy, and Turkey.

REFERENCES

[1] M. Bharathidasan, V. Indragandhi, V. Suresh, M. Jasinski, and Z. Leonowicz, "A review on electric vehicle: Technologies, energy trading, and cyber security," *Energy Rep.*, vol. 8, pp. 9662–9685, Nov. 2022.
[2] "European network of transmission system operators for electricity (ENTSO-E)," ENTSO-E, Brussels, Belgium, Annu. Rep., 2022.
[3] J. A. Sanguesa, V. Torres-Sanz, P. Garrido, F. J. Martinez, and J. M. Marquez-Barja, "A review on electric vehicles: Technologies and challenges," *Smart Cities*, vol. 4, pp. 372–404, Mar. 2021.
[4] *International Energy Agency*, Global EV Outlook, Paris, France, 2023.
[5] *United States Driving Research and Innovation for Vehicle Efficiency and Energy Sustainability (U.S. DRIVE)*, Elect. Electron. Tech. Team Roadmap, Washington, DC, USA, 2017.
[6] *European Road Transport Research Advisory Council (ERTRAC), European Platform on Smart Systems (EPoSS), European Technology & Innovation Platforms Strategic Energy Technology (ETIPs SNET)*, Eur. Roadmap Electrific. Road Transp., Brussels, Belgium, 2017.
[7] K. P. Maroti, S. Padmanaban, M. S. Bhaskar, V. K. Ramachandaramurthy, and F. Blaabjerg, "The state-of-the-art of power electronics converters configurations in electric vehicle technologies," *Power Electron. Devices Compon.*, vol. 1, Mar. 2022, Art. no. 100001.
[8] I. Husain, B. Ozpineci, M. S. Islam, E. Gurpinar, G.-J. Su, W. Yu, S. Chowdhury, L. Xue, D. Rahman, and R. Sahu, "Electric drive technology trends, challenges, and opportunities for future electric vehicles," *Proc. IEEE*, vol. 109, no. 6, pp. 1039–1059, Jun. 2021.
[9] Y.-G. Lv, G.-P. Zhang, Q.-W. Wang, and W.-X. Chu, "Thermal management technologies used for high heat flux automobiles and aircraft: A review," *Energies*, vol. 15, no. 21, pp. 1–39, 2022.
[10] Y. Yang, L. Dorn-Gomba, R. Rodriguez, C. Mak, and A. Emadi, "Automotive power module packaging: Current status and future trends," *IEEE Access*, vol. 8, pp. 160126–160144, 2020.
[11] D. Garrido-Diez and I. Baraia, "Review of wide bandgap materials and their impact in new power devices," in *Proc. IEEE Int. Workshop Electron., Control, Meas., Signals Appl. Mechatronics (ECMSM)*, May 2017, pp. 1–6.
[12] L. Zhang, Z. Zheng, and X. Lou, "A review of WBG and Si devices hybrid applications," *Chin. J. Electr. Eng.*, vol. 7, no. 2, pp. 1–20, Jun. 2021.
[13] Y. Xiong, A. Oyane, T. Ou, S. Thilak, J. Imaoka, and M. Yamamoto, "Comparison of switching performance between GaN and SiC MOSFET via 13.56 MHz half-bridge inverter," in *Proc. IEEE 29th Int. Symp. Ind. Electron. (ISIE)*, Delft, The Netherlands, Jun. 2020, pp. 634–638.
[14] R. T. Yadlapalli, A. Kotapati, R. Kandipati, S. R. Balusu, and C. S. Koritala, "Advancements in energy efficientGaNpower devices and power modules for electric vehicle applications: A review," *Int. J. Energy Res.*, vol. 45, no. 9, pp. 12638–12664, Jul. 2021.
[15] A. Allca-Pekarovic, P. J. Kollmeyer, P. Mahvelatishamsabadi, T. Mirfakhrai, P. Naghshtabrizi, and A. Emadi, "Comparison of IGBT and SiC inverter loss for 400 V and 800 V DC bus electric vehicle drivetrains," in *Proc. IEEE Energy Convers. Congr. Expo. (ECCE)*. Detroit, MI, USA: Institute of Electrical and Electronics Engineers, Oct. 2020, pp. 6338–6344.
[16] W. Perdikakis, M. J. Scott, K. J. Yost, C. Kitzmiller, B. Hall, and K. A. Sheets, "Comparison of Si and SiC EMI and efficiency in a two-level aerospace motor drive application," *IEEE Trans. Transport. Electrific.*, vol. 6, no. 4, pp. 1401–1411, Dec. 2020.
[17] Y. Wu, M. J. Hoque, M. H. Mahmud, E. M. Allee, A. A. Lad, Y. Zhao, H. A. Mantooth, and N. Miljkovic, "Electrothermal-control co-design of an all silicon carbide 2×250 kW dual inverter for heavy-duty traction applications," *IEEE Trans. Ind. Appl.*, vol. 58, no. 1, pp. 505–516, Jan. 2022.
[18] C. Zhang, S. Srdic, S. Lukic, K. Sun, J. Wang, and R. Burgos, "A SiC-based liquid-cooled electric vehicle traction inverter operating at high ambient temperature," *CPSS Trans. Power Electron. Appl.*, vol. 7, no. 2, pp. 160–175, Jun. 2022.
[19] X. Zhang, X. L. Zhao, W. Li, Z. Wang, A. Liao, Y. Song, Y. Wang, and L. Zhang, "Ultra-thermostable embedded liquid cooling in SiC 3D packaging power modules of electric vehicles," *Energy Convers. Manag.*, vol. 276, Jul. 2023, Art. no. 116499.
[20] *Inverter Generation 4*, BOSCH, Gerlingen, Germany, 2022.
[21] G. Iannaccone, C. Sbrana, I. Morelli, and S. Strangio, "Power electronics based on wide-bandgap semiconductors: Opportunities and challenges," *IEEE Access*, vol. 9, pp. 139446–139456, 2021.
[22] C. Tan, M. Stecca, T. B. Soeiro, J. Dong, and P. Bauer, "Performance evaluation of an electric vehicle traction drive using Si/SiC hybrid switches," in *Proc. IEEE 19th Int. Power Electron. Motion Control Conf. (PEMC)*, Gliwice, Poland, Apr. 2021, pp. 278–283.
[23] C. Ding, H. Liu, K. D. T. Ngo, R. Burgos, and G.-Q. Lu, "A double-side cooled SiC MOSFET power module with sintered-silver interposers: I-design, simulation, fabrication, and performance characterization," *IEEE Trans. Power Electron.*, vol. 36, no. 10, pp. 11672–11680, Oct. 2021.
[24] G. Moreno, S. Narumanchi, X. Feng, P. Anschel, S. Myers, and P. Keller, "Electric-drive vehicle power electronics thermal management: Current status, challenges, and future directions," *J. Electron. Packag.*, vol. 144, no. 1, pp. 1–11, Mar. 2022.
[25] Y. Qin, B. Albano, J. Spencer, J. S. Lundh, B. Wang, C. Buttay, M. Tadjer, C. DiMarino, and Y. Zhang, "Thermal management and packaging of wide and ultra-wide bandgap power devices: A review and perspective," *J. Phys. D, Appl. Phys.*, vol. 56, no. 9, Mar. 2023, Art. no. 093001.
[26] Z. Zeng, K. Ou, L. Wang, and Y. Yu, "Reliability-oriented automated design of double-sided cooling power module: A thermo-mechanical-coordinated and multi-objective-oriented optimization methodology," *IEEE Trans. Device Mater. Rel.*, vol. 20, no. 3, pp. 584–595, Sep. 2020.
[27] C. Peng, Q. Huang, F. Qi, P. Ke, X. Dai, W. Zhu, and L. Wang, "Investigation on the reliability of die-attach structures for double-sided cooling power module," *IEEE Trans. Compon., Packag., Manuf. Technol.*, vol. 11, no. 5, pp. 793–801, May 2021.
[28] M. Liu, A. Coppola, M. Alvi, and M. Anwar, "Comprehensive review and state of development of double-sided cooled package technology for automotive power modules," *IEEE Open J. Power Electron.*, vol. 3, pp. 271–289, 2022.
[29] P. Lu, L. Li, G.-Q. Lu, Z. Shuai, X. Guo, and Y.-H. Mei, "Review of double-sided cooling power modules for driving electric vehicles," *IEEE Trans. Device Mater. Rel.*, vol. 23, no. 2, pp. 287–296, Jun. 2023.
[30] X. Liu, M. Wei, M. Qiu, K. Hobbs, S. Yang, A. Dahneem, and D. Cao, "FPGA-based forced air-cooled SiC high-power-density inverter for electrical aircraft applications," in *Proc. IEEE Appl. Power Electron. Conf. Expo. (APEC)*, Mar. 2023, pp. 3169–3173.
[31] S. Nakata and I. Omura, "Direct/indirect impinging air jet cooling for power devices and application to power electronics system," in *Proc. 12th Int. Conf. Integr. Power Electron. Syst.*, Mar. 2022, pp. 1–6.
[32] P. Sahoo, "A review on immersion cooling for power electronics," SAE, Tech. Paper 2022-28-0446, pp. 1–6, 2022, doi: 10.4271/2022-28-0446.
[33] H. Wei, C. Biao, L. Huitao, L. Guangkun, and Y. Jiayi, "Research on phase change cooling technology of vehicle fraction converter module," in *Proc. IEEE 5th Int. Electr. Energy Conf. (CIEEC)*, Nangjing, China, May 2022, pp. 397–403.
[34] E. Abramushkina, A. Zhaksylyk, T. Geury, M. El Baghdadi, and O. Hegazy, "A thorough review of cooling concepts and thermal management techniques for automotive WBG inverters: Topology, technology and integration level," *Energies*, vol. 14, no. 16, p. 4981, Aug. 2021.
[35] *BOYD's Innovative Solutions Enable Disruptive Technologies and Leading Customers in High Growth, High Innovation Industries: eMobility*, BOYD, Pleasanton, CA, USA.
[36] K. Deepak, M.-T. Tran, D.-D. Tran, M. El Baghdadi, and O. Hegazy, "Design investigation of liquid cooled heat sink for GaN FET dual-three phase inverter," in *Proc. Int. Symp. Power Electron., Electr. Drives, Autom. Motion (SPEEDAM)*, Jun. 2022, pp. 149–154.
[37] P. H. A. S. E. Silva, E. C. da Silva, L. R. Rocha, P. R. Eckert, and R. P. Vieira, "Analysis and modeling of a liquid cooled heat sink for EV traction inverter systems," in *Proc. IEEE Transp. Electrific. Conf. Expo (ITEC)*, CA, CA, USA, Jun. 2022, pp. 825–830.
[38] G. Ghaisas and S. Krishnan, "A critical review and perspective on thermal management of power electronics modules for inverters and converters," *Trans. Indian Nat. Acad. Eng.*, vol. 7, no. 1, pp. 47–60, Mar. 2022.
[39] S. Jones-Jackson, R. Rodriguez, Y. Yang, L. Lopera, and A. Emadi, "Overview of current thermal management of automotive power electronics for traction purposes and future directions," *IEEE Trans. Transport. Electrific.*, vol. 8, no. 2, pp. 2412–2428, Jun. 2022.
[40] Z. Shuai, S. He, Y. Xue, Y. Zheng, J. Gai, Y. Li, G. Li, and J. Li, "Junction temperature estimation of a SiC MOSFET module for 800 V high-voltage application in electric vehicles," *eTransportation*, vol. 16, Apr. 2023, Art. no. 100241.

[41] O. Tayyara, J. Palumbo, N. Khan, M. Nasr, C. Da Silva, S. Chandra, O. Trescases, and C. H. Amon, "Miniature liquid cold-plate enabled by metal spraying: A thermal management solution for a modular 1 kW bi-directional GaN-based DC–AC converter," in *Proc. IEEE Appl. Power Electron. Conf. Expo. (APEC)*, Houston, TX, USA, Mar. 2022, pp. 312–318.

[42] S. Lau. *Liquid Cold Plate Introduction & Production Process*. Accessed: Aug. 18, 2023. [Online]. Available: https://www.linkedin.com/pulse/liquid-cold-plate-introduction-production-process-sam-lau/

[43] R. C. Panati, F. Alpiovezza, G. De Luca, and G. Francesconi, "Cooling channel optimization in power inverter design," in *Proc. IEEE 20th Int. Power Electron. Motion Control Conf. (PEMC)*, Brasov, Romania, Sep. 2022, pp. 1–6.

[44] M. Shahjalal, T. Shams, S. B. Hossain, M. R. Ahmed, M. Ahsan, J. Haider, R. Goswami, S. B. Alam, and A. Iqbal, "Thermal analysis of Si-IGBT based power electronic modules in 50 kW traction inverter application," *e-Prime-Adv. Electr. Eng., Electron. Energy*, vol. 3, Mar. 2023, Art. no. 100112.

[45] *Extruded Micro-Channel Liquid Cold Plates for Cooling Power Electronics and Battery Packs*, Bankor, Mississauga, ON, Canada.

[46] I. Kaur and P. Singh, "State-of-the-art in heat exchanger additive manufacturing," *Int. J. Heat Mass Transf.*, vol. 178, Oct. 2021, Art. no. 121600.

[47] L. Lopera, R. Rodriguez, M. Yakout, M. Elbestawi, and A. Emadi, "Current and potential applications of additive manufacturing for power electronics," *IEEE Open J. Power Electron.*, vol. 2, pp. 33–42, 2021.

[48] N. Gilmore, V. Timchenko, and C. Menictas, "Manifold microchannel heat sink topology optimisation," *Int. J. Heat Mass Transf.*, vol. 170, May 2021, Art. no. 121025.

[49] C. U. Gonzalez-Valle, S. Samir, and B. Ramos-Alvarado, "Experimental investigation of the cooling performance of 3-D printed hybrid water-cooled heat sinks," *Appl. Thermal Eng.*, vol. 168, Mar. 2020, Art. no. 114823.

[50] F. Han, H. Guo, and X. Ding, "Design and optimization of a liquid cooled heat sink for a motor inverter in electric vehicles," *Appl. Energy*, vol. 291, Jun. 2021, Art. no. 116819.

[51] L. E. Paniagua-Guerra, S. Sehgal, C. U. Gonzalez-Valle, and B. Ramos-Alvarado, "Fractal channel manifolds for microjet liquid-cooled heat sinks," *Int. J. Heat Mass Transf.*, vol. 138, pp. 257–266, Aug. 2019.

[52] A. J. Robinson, R. Kempers, J. Colenbrander, N. Bushnell, and R. Chen, "A single phase hybrid micro heat sink using impinging micro-jet arrays and microchannels," *Appl. Thermal Eng.*, vol. 136, pp. 408–418, May 2018.

[53] Y. Xia, L. Chen, J. Luo, and W. Tao, "Numerical investigation of microchannel heat sinks with different inlets and outlets based on topology optimization," *Appl. Energy*, vol. 330, Jan. 2023, Art. no. 120335.

[54] C.-W. Chang, X. Zhao, R. Phukan, D. Dong, R. Burgos, and A. Plat, "Weight-minimizing optimization of microchannel cold plate for sic-based power inverters in more-electric aircraft," in *Proc. IEEE Energy Convers. Congr. Expo. (ECCE)*, Detroit, MI, USA, Oct. 2022, pp. 1–8.

[55] X. L. Wu, C. Y. Li, J. L. Yang, Y. Liu, and X. H. Han, "Theoretical and experimental research on flow boiling heat transfer in microchannels for IGBT modules," *Int. J. Heat Mass Transf.*, vol. 205, May 2023, Art. no. 123900.

[56] C. Chen, L. Yi, and M. Pan, "Optimization and experimental verification of microchannel heat sink based on heat transfer and flow balance regulation," *Chem. Eng. J.*, vol. 455, Jan. 2023, Art. no. 140793.

[57] P. S. Ghahfarokhi, A. Podgornovs, A. Kallaste, A. J. M. Cardoso, A. Belahcen, T. Vaimann, H. Tiismus, and B. Asad, "Opportunities and challenges of utilizing additive manufacturing approaches in thermal management of electrical machines," *IEEE Access*, vol. 9, pp. 36368–36381, 2021.

[58] M. Javaid, A. Haleem, R. P. Singh, R. Suman, and S. Rab, "Role of additive manufacturing applications towards environmental sustainability," *Adv. Ind. Eng. Polym. Res.*, vol. 4, no. 4, pp. 312–322, Oct. 2021.

[59] S. Mooraj, Z. Qi, C. Zhu, J. Ren, S. Peng, L. Liu, S. Zhang, S. Feng, F. Kong, Y. Liu, E. B. Duoss, S. Baker, and W. Chen, "3D printing of metal-based materials for renewable energy applications," *Nano Res.*, vol. 14, no. 7, pp. 2105–2132, Jul. 2021.

[60] J. C. Najmon, S. Raeisi, and A. Tovar, "Review of additive manufacturing technologies and applications in the aerospace industry," in *Additive Manufacturing for the Aerospace Industry*. Amsterdam, The Netherlands: Elsevier, 2019, pp. 7–31.

[61] J. Lie. *Automotive Industry Supports Additive Manufacturing*. Accessed: Aug. 16, 2023. [Online]. Available: https://www.runsom.com/ and https://www.runsom.com/blog/automotive-industry-supports-additive-manufacturing/

[62] D. Schuhmann, C. Rockinger, M. Merkel, and D. K. Harrison, "A study on additive manufacturing for electromobility," *World Electric Vehicle J.*, vol. 13, no. 8, p. 154, Aug. 2022.

[63] R. Miozga and M. Kurek, "Effect of print orientation using DMLS method on strength of materials," in *Proc. MATEC Web Conf.*, vol. 338, Jun. 2021, p. 01017.

[64] C. B. Dokken and B. M. Fronk, "Optimization of 3D printed liquid cooled heat sink designs using a micro-genetic algorithm with bit array representation," *Appl. Thermal Eng.*, vol. 143, pp. 316–325, Oct. 2018.

[65] Y. A. Manaserh, A. R. Gharaibeh, M. I. Tradat, S. Rangarajan, B. G. Sammakia, and H. A. Alissa, "Multi-objective optimization of 3D printed liquid cooled heat sink with guide vanes for targeting hotspots in high heat flux electronics," *Int. J. Heat Mass Transf.*, vol. 184, Mar. 2022, Art. no. 122287.

[66] A. A. Lad, M. J. Hoque, S. Christian, Y. Zhao, J. C. Balda, W. P. King, and N. Miljkovic, "High power density thermal management of discrete semiconductor packages enabled by additively manufactured hybrid polymer-metal coolers," *Appl. Thermal Eng.*, vol. 220, Feb. 2023, Art. no. 119726.

[67] S. Ozguc, T. F. G. Teague, L. Pan, and J. A. Weibel, "Experimental study of topology optimized, additively manufactured microchannel heat sinks designed using a homogenization approach," *Int. J. Heat Mass Transf.*, vol. 209, Aug. 2023, Art. no. 124108.

[68] J. Tompkins and D. Huitink, "Air flow inversion for enhanced electronics cooling in additively manufactured air channels," in *Proc. 19th IEEE Intersociety Conf. Thermal Thermomechanical Phenomena Electron. Syst. (ITherm)*, Orlando, FL, USA, Jul. 2020, pp. 734–739.

[69] R. Whitt, Z. Yuan, A. I. Emon, F. Luo, and D. Huitink, "Electrothermal system design and evaluation of low EMI and thermally balanced 150 kW T-type traction inverter," *IEEE Trans. Power Electron.*, vol. 38, no. 1, pp. 538–547, Jan. 2023.

[70] A. P. Pai, M. Ebli, T. Simmet, A. Lis, and M. Beninger-Bina, "Characteristics of a SiC MOSFET-based double side cooled high performance power module for automotive traction inverter applications," in *Proc. IEEE Transp. Electrific. Conf. Expo (ITEC)*, Benin, Jun. 2022, pp. 831–836.

[71] S. Jones-Jackson, R. Rodriguez, and A. Emadi, "Jet impingement cooling in power electronics for electrified automotive transportation: Current status and future trends," *IEEE Trans. Power Electron.*, vol. 36, no. 9, pp. 10420–10435, Sep. 2021.

[72] S. Moeller, D. Karimi, O. Vanegas, M. El Baghdadi, A. Kospach, A. Lis, B. Rabl, O. Hegazy, and C. Abart, "Application considerations for double sided cooled modules in automotive environment," in *Proc. 11th Int. Conf. Integr. Power Electron. Syst.*, Mar. 2020, pp. 1–7.

[73] H. Rasool, B. Verbrugge, S. Jaman, E. Abramushkina, T. Geury, M. El Baghdadi, and O. Hegazy, "Design and real-time implementation of a control system for SiC off-board chargers of battery electric buses," *Energies*, vol. 15, no. 4, p. 1434, Feb. 2022.

EKATERINA E. ABRAMUSHKINA received the B.S. and M.S. degrees in power electronics engineering from Novosibirsk State Technical University (NSTU), Novosibirsk, Russia, in 2016 and 2018, respectively. She is currently pursuing the Ph.D. degree in engineering sciences with the MOBI Electromobility Research Centre, Vrije Universiteit Brussel, Brussels, Belgium.

From 2018 to 2020, she was a half-time Research Assistant with NSTU and a half-time Power Electronic Design Engineer in the mining industry with a focus on control systems for electric drives. Her research interest includes the development of a power train for an electric vehicle, power electronics converters design, and control.

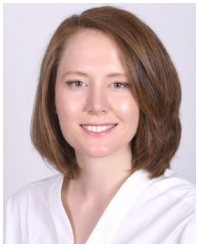

GAMZE EGIN MARTIN received the bachelor's and master's degrees in mechanical engineering from Uludag University, Bursa, Turkey. She is currently pursuing the Ph.D. degree in electrical engineering and energy technology with Vrije Universiteit Brussel (VUB), Brussels, Belgium.

She is a Ph.D. Researcher with the MOBI-Efficient Power Electronics, Powertrain, and Energy Solutions (EPOWERS) Research Group, VUB. With an extensive background in the industry for more than five years, she has honed her expertise in the automotive and optoelectronic sectors, particularly in the research and development domain. In her prior role as a Research and Development Project Responsible with Renault Group, Turkey, she played a role in project management and product development. Her research interests include thermal management for power electronics systems in automotive applications, bridging the realms of energy efficiency, and sustainable transportation.

ATILA SEN received the B.S. and M.S. degrees in industrial engineering from the MOBI, Vrije Universiteit Brussel, Brussels, Belgium, in 2021 and 2023, respectively.

Since 2023, he has been a Qualification Engineer with Tractebel, Brussels. His research interests include the development of designs for 3D printing, ANSYS® Fluent CFD virtual prototypes, and power trains for electric vehicles.

SHAHID JAMAN (Member, IEEE) received the B.Sc. degree in electrical and electronic engineering (EEE) from the Ahsanullah University of Science and Technology, Dhaka, Bangladesh, in 2011, and the joint M.Sc. degree in Erasmus mundus master course and in sustainable transportation and electrical power systems (STEPS), in 2017.

He is currently a Ph.D. Researcher with the Efficient Power Electronics, Powertrain, and Energy Solutions (EPOWERS) Research Group, Department of Electrical Machines and Energy Technology (ETEC), and the MOBI Research Centre, Vrije Universiteit Brussels, Belgium. He is also involved in the European projects (eCharge4Driver and NextERUCK). His research interests include modeling, design, and control of power electronics converters based on wide band gap (WBG) technologies for light-duty and medium-duty vehicles, microgrid/nanogrid modeling and validation, simulation design, stability, real-time systems, prototyping, control, design, and optimization.

HAARIS RASOOL received the B.E. degree in electrical engineering from Air University, Islamabad, Pakistan, in 2012, the M.S. degree in electrical engineering from FAST NUCES, Islamabad, in 2016, and the Ph.D. degree in engineering sciences from the Department of Electrical Machines and Energy Technology (ETEC) and the MOBI Research Centre, Vrije Universiteit Brussels (VUB), Brussels, Belgium, in 2023.

His professional experience includes serving as a Research Associate with FAST NUCES, Islamabad, from 2013 to 2014, the Department Manager in Control System Design with Research and Development Organization, Islamabad, from 2014 to 2018, and a Ph.D. and Postdoctoral Researcher specializing in power converters design and development for EVs with EPOWERS Research Group, Department of ETEC, and the MOBI Research Centre, VUB. He is currently the Product Manager in power converters for railway with ABB, Berlin, Germany.

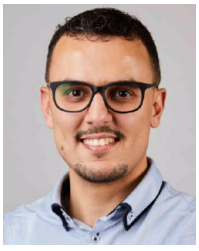

MOHAMED EL BAGHDADI (Member, IEEE) received the M.Sc. degree in electromechanical engineering and the Ph.D. degree in engineering sciences from Vrije Universiteit Brussel (VUB), Belgium, in 2009.

After M.Sc. degree, his research focused on control engineering in steel manufacturing's hot-strip rolling process. Since 2011, his research has focused on electric and hybrid vehicles, drivetrain modeling and testing, and wireless charging systems, while contributing to numerous national and European research projects in these fields and working as an Academic Teaching Assistant. Since 2018, he has been a Postdoctoral Researcher in power electronics, electric machines, and (hybrid) electric vehicle powertrains with the MOBI research Centre, VUB, where he currently leads the vehicle powertrain team and a Professor associated with the Department of Electrical Engineering and Energy Technology. He is involved in teaching electrical engineering courses in academia and industry. He is also the Co-Director of the Efficient Power Electronics, Powertrain and Energy Solutions (EPOWERS) Research Group, acting as the Manager of the MOBI Core Laboratory within Flanders Make, and a member of the European Power Electronics (EPE) Association. His activities include research and management of national and international projects in the domains of power electronics, electric machines, electric and hybrid vehicle powertrains, and (wireless) charging. His main research interests include power and energy management strategies and control, design, and optimization, (digital twin) simulation, and system testing.

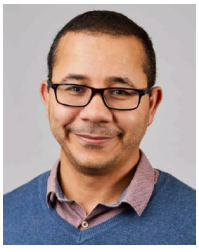

OMAR HEGAZY (Member, IEEE) received the Ph.D. degree (Hons.) from the Department of Electrical Machines and Energy Technology (ETEC), Vrije Universiteit Brussel (VUB), Belgium, in July 2012.

He is currently the Head of the Efficient Power Electronics, Powertrain and Energy Solutions (EPOWERS) Research Group, Department of ETEC, and the MOBI Research Centre, VUB, where he coordinates the research activities in this field in several national projects (e.g., via Flanders Make VLAIO (ex. IWT), Innoviris, and Flux50) and European projects (e.g., SAFEDRIVE, UNPLUGGED, ELIPTIC, ORCA, ASSURED, HiFi-Elements, GHOST, HiPERFORM, ACHILES, LONGRUN, eCharge4drivers, iSTORMY, URBANIZED, ASSURED, HiEFFICIENT, SiC4GRID, NEMOSHIP, NextERUCK, EcoMobility, and ZEEFES). He is the author of more than 140 scientific publications and two patent applications. His research interests include power electronics, electrical machines, electric and (plug-in) hybrid electric vehicles, digital twins (DTs), charging infrastructure, power/energy management strategies, battery management systems (BMSs), V2X systems, and optimization techniques and smart DC grid with renewable energy. He is a member of EPE and IEC standards.